Caliste 64, an Innovative CdTe Hard X-Ray Micro-Camera

A. Meuris, O. Limousin, F. Lugiez, O. Gevin, F. Pinsard, I. Le Mer, E. Delagnes, M. C. Vassal, F. Soufflet, and R. Bocage

***Abstract*—A prototype 64 pixel miniature camera has been designed and tested for the Simbol-X hard X-ray observatory to be flown on the joint CNES-ASI space mission in 2014. This device is called Caliste 64. It is a high performance spectro-imager with event time-tagging capability, able to detect photons between 2 keV and 250 keV. Caliste 64 is the assembly of a 1 or 2 mm thick CdTe detector mounted on top of a readout module. CdTe detectors equipped with Aluminum Schottky barrier contacts are used because of their very low dark current and excellent spectroscopic performance. Front-end electronics is a stack of four IDeF-X V1.1 ASICs, arranged perpendicular to the detection plane, to read out each pixel independently. The whole camera fits in a $10 \times 10 \times 20$ mm^3 volume and is juxtaposable on its four sides. This allows the device to be used as an elementary unit in a larger array of Caliste 64 cameras. Noise performance resulted in an ENC better than 60 electrons rms in average. The first prototype camera is tested at $-10°\mathrm{C}$ with a bias of -400 V. The spectrum summed across the 64 pixels results in a resolution of 697 eV FWHM at 13.9 keV and 808 eV FWHM at 59.54 keV.**

***Index Terms*—ASIC, CdTe, IDeF-X, Simbol-X, spectroscopy, X-ray astronomy detectors, X-ray image sensors.**

I. Introduction

THE Simbol-X space mission, currently undergoing a joint CNES-ASI phase A, is a hard X-ray telescope project involving two satellites flying in formation [1]. One satellite carries a grazing incidence mirror [2] while the other holds the detector payload. The mission aims at studying high energy phenomena in the universe such as matter accretion near black holes. The X-ray focusing technique requires specific constraints on the detection instruments. On one hand, a pixel pitch of 625 μm is necessary to sample the 1 cm^2 point spread function. On the other hand, the specified 12 arcmin field of view requires a detector array of 64 cm^2. Detector material uniformity is also essential to guarantee high imaging quality.

The Simbol-X focal plane is an assembly of three compact detector units. The low energy detector is based on the DEPFET technology [3] and covers the energy range from 0.5 to 20 keV. The high energy detector (HED) is efficient from 8 to 100 keV. The third unit is an active shield to reject the background [4].

The HED will be a mosaic of independent 256-pixel miniature cameras, featuring Cadmium Telluride (CdTe) detectors with segmented electrodes and full custom front-end ASIC named IDeF-X. CdTe is a semiconductor well suited for X and gamma rays detection, with excellent properties for imaging and spectroscopy. Contrary to silicon, a 2 mm-thick CdTe detector is still 97% efficient at 80 keV. Contrary to germanium, it can be processed with small pixel sizes for imaging and it can be easily operated at room temperature or moderately cooled. The spectroscopic performance baseline for the mission is a mean resolution of 1.3 keV FWHM at 60 keV over the whole detection plane (16384 channels). That requires very low noise front-end electronics.

The first step of the HED development is a prototype 64-pixel miniature camera named Caliste 64. Section II describes the Caliste 64 design based on a 3D-technology mastered by the 3D Plus company (France). Section III presents performance of new Schottky CdTe detectors manufactured by Acrorad (Japan) [5] and characterization of Caliste 64 electronics. First results with a fully integrated Caliste 64 camera are presented in Section IV.

II. Caliste 64 Design

Caliste 64 incorporates a hybrid detector-readout design. The purpose of hybridization is to integrate a 64-pixel CdTe crystal with its front-end electronics into single component. Four ASICs are used to read out the 64 pixels. Each ASIC is connected to two rows of eight pixels. The compact design is achieved by mounting the four ASICs boards perpendicularly below the detection surface, as illustrated in the X-ray radiography (Fig. 1). The ASIC stack is a $10 \times 10 \times 18$ mm^3 3D-module, designed and fabricated according to the 3D Plus technology [6]. It is called Caliste 64 electrical body since it only integrates the front-end electronics part of the camera.

The design of Caliste 64 was optimized to fulfill requirements for space devices related to power consumption, radiation hardness and environmental constraints (including thermal cycles, vibration and shock). The following paragraphs describe the constitutive elements and the fabrication process of the camera.

A. CdTe Detectors

The detector anode is an 8×8 array of 900 μm pixels. The pixels are separated by a 100 μm gap, and are surrounded by a 900 μm guard ring. The planar cathode is platinum, and the

Manuscript received November 15, 2007; revised January 25, 2008. This work was supported by CNES (French National Space Agency).

A. Meuris, O. Limousin, F. Pinsard, and I. Le Mer are with CEA Saclay/DSM/DAPNIA Service d'Astrophysique, 91191 Gif-sur-Yvette, France (e-mail: aline.meuris@cea.fr).

F. Lugiez, O. Gevin, and E. Delagnes are with the CEA Saclay/DSM/DAPNIA Service d'Electronique, 91191 Gif-sur-Yvette, France.

M. C. Vassal, F. Soufflet, and R. Bocage are with the 3D-plus Company, 78532 BUC, France (e-mail: mcvassal@3d-plus.com).

Color versions of one or more of the figures in this paper are available online at http://ieeexplore.ieee.org.

Digital Object Identifier 10.1109/TNS.2008.918742

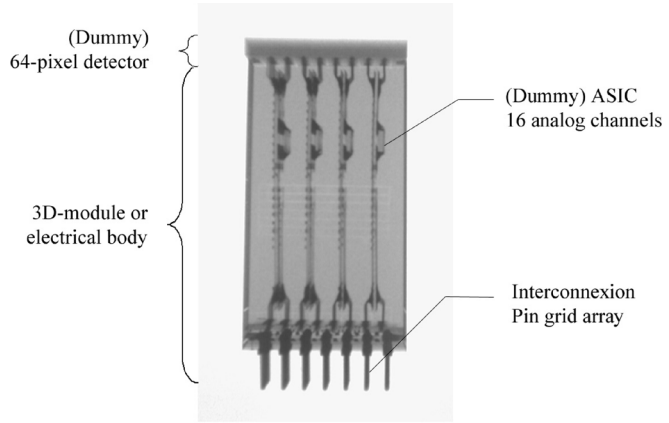

Fig. 1. X-ray radiography of a dummy Caliste 64 device with a dummy detector and dummy chips. The Caliste 64 camera consists of a 1 or 2 mm-thick CdTe detector with 64 pixels and a $10 \times 10 \times 18\ \mathrm{mm}^3$ 3D-module called electrical body.

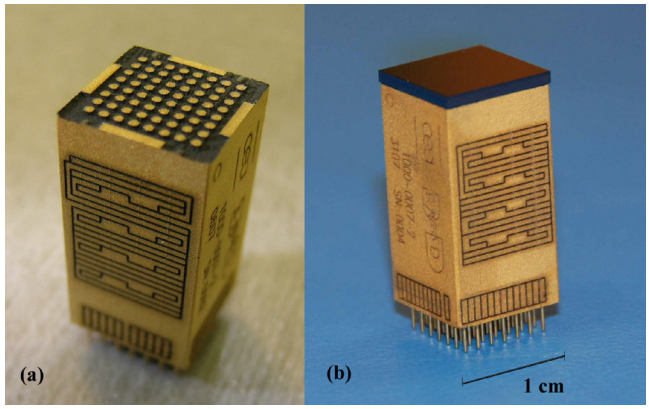

Fig. 2. (a) The $10 \times 10 \times 18\ \mathrm{mm}^3$ Caliste 64 electrical body, including four stacked IDeF-X V1.1 ASICs. The top surface of the 3D-module is prepared by laser ablation to receive the 64-pixel detector. (b) First prototype of Caliste 64 camera. Each pixel of the CdTe Schottky detector is connected individually to its readout channel input. The 49-pin PGA is visible at the bottom, as well as the signal routing on lateral surfaces.

anode electrodes are aluminum-titanium-gold [7], [8]. The difference in work function between aluminum and cadmium telluride is responsible for creating a Schottky barrier contact on the collection electrode [9]. When reverse biased, the contact is blocking, which leads to a very low dark current. In contrast to indium contacts, Schottky contacts containing aluminum support photolithography processes efficient at achieving small pixels.

B. ASIC IDeF-X V1.1

The ASIC used in Caliste 64 is called IDeF-X V1.1 and was designed for X-rays detection in space environment [10]. The chip is a low noise (ENC 35 el. rms at 0 pF load, no detector current), low power (3 mW per channel) and radiation hard (up to 1 MRad) analog circuit. The ASIC is self triggered and delivers a signal level proportional to the energy deposit in the detector. An individual channel consists of a low noise charge sensitive preamplifier, a pole-zero cancellation stage, a fourth order Sallen & Key type shaper with adjustable peaking time and a peak detection system followed by an analog memory to store the magnitude of the resulting pulse height. The analog memories are multiplexed to the single ended output multiplexer (16:1). Each channel integrates a discriminator with an adjustable low level threshold which is common to the 16 channels.

C. Hybrid Fabrication

The ASICs are mounted by classical wire bonding on mini printed circuits boards (PCB) substrates. The latter must have good dielectric properties to avoid excess of noise due to dielectric losses. The design is done such a way to limit parasitic capacitances and consequently, series and $1/\mathrm{f}$ noise. The residual parasitic capacitance is estimated to be near 1 pF, without the CdTe pixel self capacitance. The four PCB substrates are stacked and molded inside an insulating epoxy resin according to the 3D Plus technology. The resulting block is diced and metallized. The top surface of the block is prepared by laser ablation to receive a $1\ \mathrm{cm}^2$ matrix of 8×8 pixels. Each pixel pad is connected to an ASIC input. An interconnection stack drives signals from the main block to the bottom 7×7 pin grid array, 1.27 mm pitch. Finally, a $10 \times 10 \times 1\ \mathrm{mm}^3$ CdTe detector is fixed using a polymer bump bonding technique at a moderate curing temperature, to obtain the Caliste 64 camera.

The bottom interface is minimized to 49 pins including analog and digital pins, power supplies, ground and ASICs output pins. This design allows easy routing of an array of Caliste 64 units placed side by side. The reduction of output signals is made possible by sharing signals between ASICs. The common signals are routed together using the lateral surfaces of Caliste 64. The routing is realized by laser ablation process according to 3D Plus technology, as shown in Fig. 2. Single and differential analog signals are routed according specific rules in order to limit parasitic coupling with digital signals for instance.

III. Characterization of Caliste 64 Sub-Assemblies

A. Stand-Alone CdTe Schottky Detectors

Aluminum Schottky detectors are first tested separately with dedicated set-ups. Detector characterization consists of measuring dark current in each pixel versus operating temperature and bias voltage. A test bench with a system of relays and a Keithley ammeter records data from the 64 pixels individually and from the guard ring [11]. Fig. 3 shows typical current map and histogram obtained with a 1 mm-thick sample array tested at $-17°\mathrm{C}$, and biased at -400 V. We notice good uniformity over 64 pixels and a low level of current. This result is consistent with the 6 other tested samples. Only one pixel is out of global statistics with 76 pA. Half of the array has a pixel current between 1 and 2 pA. Inside the guard ring, the surface of which is equivalent to 36 pixels, the current is 163 pA.

For spectroscopic characterizations, CdTe detector prototype is mounted on substrate and integrated into a thermal enclosure equipped with a $^{241}\mathrm{Am}$ source. The detector pixels are connected to four IDeF-X V1.0 ASICs [12] that read out a quarter of the matrixes each (Fig. 4). We recorded individual spectra at $0°\mathrm{C}$, $-15°\mathrm{C}$ and $-35°\mathrm{C}$, for several bias voltages, with fast

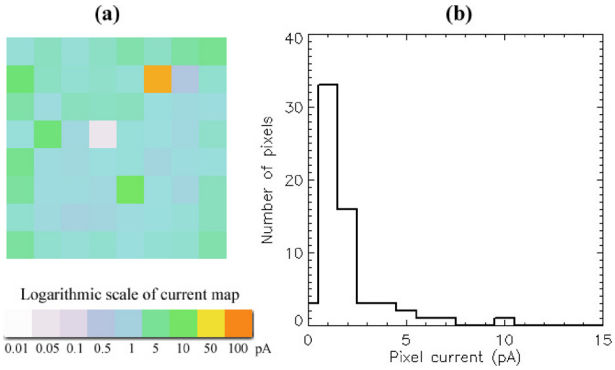

Fig. 3. Results of current measurement with a 1 mm-thick CdTe sample, at $-17°C$, -400 V. (a) Current map and its logarithmic scale in pA. (b) Histogram of currents. Half of the array has a pixel current between 1 and 2 pA.

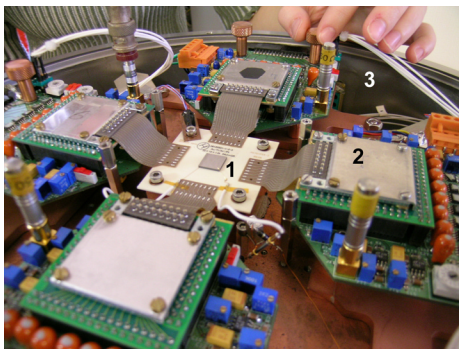

Fig. 4. Set-up of the spectroscopic measurement bench equipped with a 64-pixel CdTe detector prototype. (1) the detector mounted on a flat substrate, (2) a 16-analog channel IDeF-X V1.0 to read out a quarter of the matrix, (3) the thermal enclosure.

analog to digital converters of 512 channels per pixel. Four samples of 1 or 2 mm thick were measured and at least 63 pixels out of 64 were working well, giving good spectra when properly biased. Sum spectra are built by calibrating linearly in energy each pixel spectrum from the 13.9 keV line and the 59.54 keV line and by adding them. When the detector is cooled down to $-36°C$, sum spectrum resolution is 767 eV FWHM at 59.54 keV and 579 eV FWHM at 13.9 keV (Fig. 5). Thanks to very low dark current, bias voltage can be increased, unlike for CdTe detectors with quasi-ohmic contacts made of platinum. A mean electric field of typically 400 volts per mm limits charge loss and increases peak to valley ratio. The peak to valley ratio is computed as the ratio between counts at 59.54 keV and counts at 57 keV. For a sum spectrum, the ratio value is typically 15 for a 1 mm-thick detector and 40 for a 2 mm-thick detector.

Schottky CdTe detectors are sensitive to the polarization effect, responsible for spectral degradation during time [13]. Cooling down our detectors at $-35°C$ guarantees a good uniformity and a good stability of all the samples; spectral performance keeps unchanged during several days. As a consequence, $-35°C$ was chosen as the baseline temperature for the Simbol-X mission. However, the Al Schottky detectors can be operated at $0°C$ since spectroscopic resolution remains very satisfactory. With the same pixels and the same bias voltage as those used for Fig. 5, we get a sum spectrum resolution of 896 eV FWHM at 59.54 keV and 727 eV FWHM at 13.9 keV.

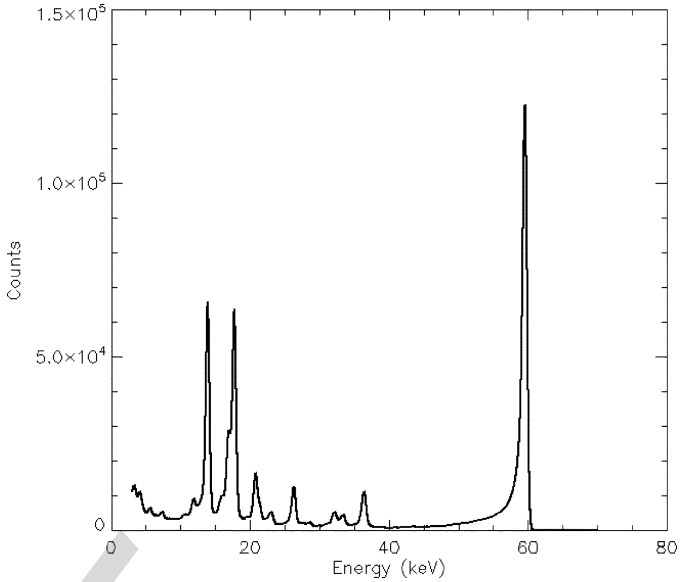

Fig. 5. Sum spectrum of an Al-Ti-Au Schottky CdTe detectors, with 63 out of 64 pixels, at $-36°C$, -400 V. Energy resolution is 579 eV FWHM at 13.9 keV and 767 eV FWHM at 59.54 keV. The peak to valley ratio between 59.54 keV and 57 keV is 14.8.

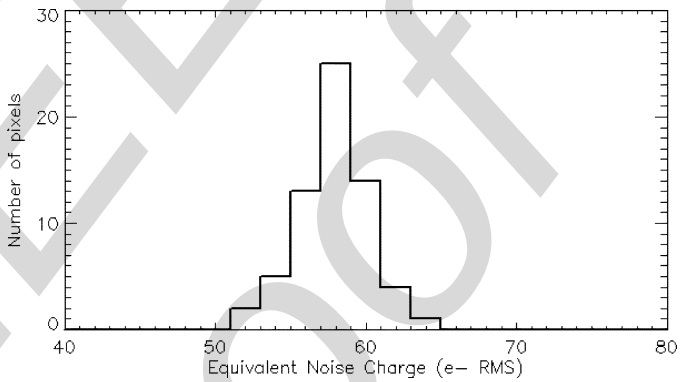

Fig. 6. Histogram of ENC for the 64 pixels of a Caliste 64 electrical body, at 9.6 μs, with a leakage current of about 3 pA.

B. Caliste 64 Electrical Body

To validate Caliste 64 electrical body shown in Fig. 2(a), we simulate the amount of charges generated in the semiconductor detector when a photon hits the material with a fast voltage step through a calibrated injection capacitance integrated inside the ASIC. The external voltage source is applied through a pin of the Caliste 64 bottom interface and is distributed to the four ASICs.

ASIC installed on their proper PCB substrates were tested before being stacked into the 3D-modules. Electronic performances are similar before and after integration. All the 64 channels operate properly, with a mean gain of 188 mV/fC for a 9.6 μs peaking time and a standard deviation of 5.1 mV/fC over the 64 channels, when leakage current is about 3 pA (typical dark current value of Fig. 3). Low noise level and uniformity are illustrated by Fig. 6. The mean equivalent noise charge (ENC) is 58.8 electrons rms and the standard deviation is 2.4 electrons rms over the 64 channels at 9.6 μs peaking time, with a leakage current of about 3 pA. That corresponds to a contribution of the electronic noise to spectral resolution of about 610 eV FWHM,

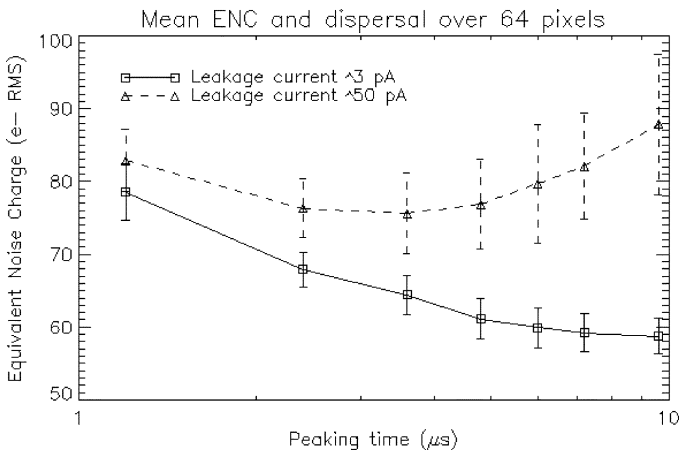

Fig. 7. ENC versus peaking time for two levels of leakage current, around 3 and 50 pA per pixel. Error bars represent standard deviation over the 64 pixels around the mean value. The optimal peaking time moves from 9.6 μs to 3.6 μs when leakage current increases.

assuming a mean electron-hole pair creation energy of 4.42 eV in CdTe. We must underline that a good uniformity was observed over the 64 pixels but also over the five electrical bodies that were realized and tested. Responses of the different samples are similar, with a mean ENC between 55 and 60 el. rms and a standard deviation between 2 and 3 el. rms over their channels, which is close to the estimated precision of this measurement.

To simulate the dark current of the detector in various conditions, a tunable current source is integrated inside the ASIC. The leakage current contributes to the parallel noise and is responsible for degrading noise performance at long peaking time values. We measure the electrical noise as function of the peaking time and the pixel dark current. From these results we can derive the optimal peaking time to use for spectroscopic tests and we can predict the spectral resolution. Results for current levels of 3 pA and 50 pA (typical values at low temperature or at room temperature respectively) are illustrated in Fig. 7. A 50 pA current leads to a noise level of 76 el. rms with a peaking time value of 3.6 μs. For currents of several pico-amps, the optimal peaking time value remains the longer peaking time (9.6 μs).

IV. Caliste 64 Performance

Following validation of electrical design and performance evaluation, we mounted detector arrays on the 3D-modules. The detector is biased using a 100 μm diameter gold wire bonded to the cathode surface. Results obtained with the first fully-integrated Caliste 64 prototype are presented in this section.

A. Caliste 64 Set-Up

The Caliste 64 devices are tested in a thermal enclosure. Data readout and storage are controlled by a Field-Programmable Gate Array (FPGA) placed outside the enclosure.

When at least one channel output reaches the threshold value, a trigger signal is sent outside the camera. The FPGA receives the trigger, records its date and processes the proper data readout sequence according to the programmed acquisition mode (full frame or hit pixels with or without their neighbor pixels). Analog data are extracted by multiplexing and encoded

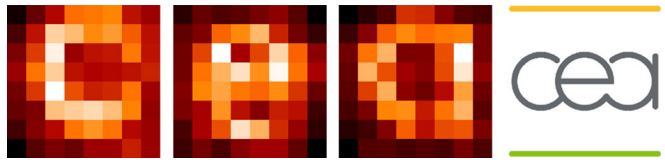

Fig. 8. Three images with Caliste 64, biased at -100 V at room temperature. The energy range is centered on 60 keV ^{241}Am line. Images were taken in one minute. Dark pixels saw about 20 photons whereas bright pixels saw about 200 photons.

by two 14-bit ADCs. Data packets are transmitted to the computer, through a Spacewire link.

As a result, each photon which hits the detector is marked as an event and is defined by its position in the matrix, its energy and its time of arrival. Caliste 64 is a spectro-imager with time-tagging capabilities. These three properties are demonstrated in the next paragraphs.

B. Imaging

The segmented anode of the detector allows an estimation of interaction position event by event. Spatial resolution is given by the pitch between pixels, 1 mm in Caliste 64. Fig. 8 shows three images performed with a ^{241}Am source to illustrate the imaging capability of Caliste 64. For easy operation and mask alignment, the detector was used at room temperature since imaging performance is not affected by the temperature, contrary to spectroscopy. We used an 11 mm-thick Tungsten collimator with an aperture of 5 mm above a 70 μm-thick Copper mask. The mask pattern is placed 13 mm from the source and about 11 mm from the detector, which leads to a magnification of about 2. Hence, letters of 2.75 mm height and 0.75 mm thick are projected 6 pixels height and 1 or 2 pixels thick.

C. Timing

The controller dates the triggering of a channel. To get the arrival time of a photon from the trigger time, one must correct time-walk, taking into account low threshold level, incident energy and peaking time. To calibrate time-walk versus incident energy, we measure the difference between the time of test injection and the triggering time, for several injection levels. By repeating this operation a high number of times, we get a random variable. Its mean value gives us the time-walk correction to apply (Fig. 9) and its standard deviation gives information on dating precision. We can see on Fig. 10 that time resolution is better than 50 ns rms for energies greater than 20 keV, when the low threshold is set to 3 keV and the peaking time is 9.6 μs. For Simbol-X mission, time-walk compensation will be implemented to perform active anticoincidence between detectors with a coincidence window of 300 ns.

Event dating in Caliste 64 enables measurement of coincidence rate and dead time. Events that hit the detector within a time window $\tau_{latency}$ (typically set to 10 μs) starting from the trigger signal, are tagged in coincidence in Caliste 64 telemetry. The most probable case is a multiple pixel trigger due to charge sharing – when a photon interacts in-between two pixels, or because an X-ray fluorescence photon escapes one pixel and stops in the neighbor. For each trigger, the sum of the energies recorded in the two pixels must give information about the

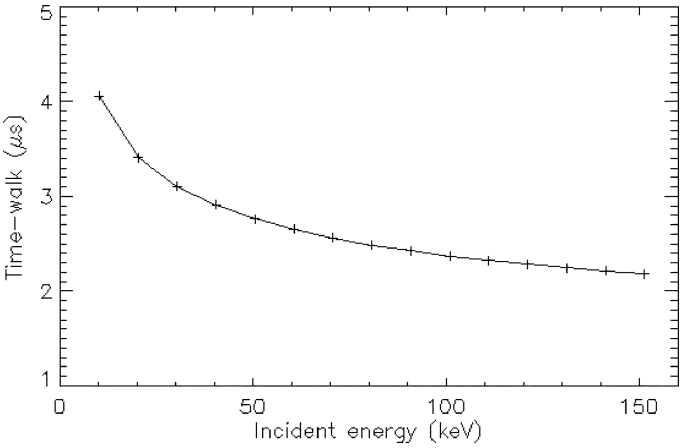

Fig. 9. Estimation of time-walk correction to apply versus energy for a low threshold of 3 keV and a peaking time of 9.6 μs. Values correspond to the mean value of the random value *Time-walk*.

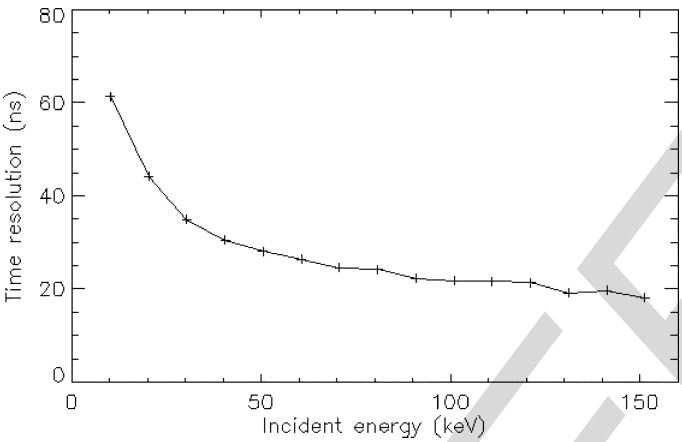

Fig. 10. Time resolution versus energy, for a low threshold of 3 keV and a peaking time of 9.6 μs. Values correspond to the standard deviation of the random value *Time-walk*.

incident photon energy deposition. The second less probable coincidence case occurs when two independent photons interact in two pixels within the system's resolving time (chance coincidence). With time tagging, we estimate that 9.2% of the events detected are in coincidence, 8.5% corresponds to neighbor pixels and 0.7% are fortuitous events (for a count rate of ~ 400 events per second).

When a trigger is detected, the Caliste 64 camera is disabled during a short time to achieve the reading sequence. This dead time depends on:

— the latency time $\tau_{latency}$ between the trigger and the peak detectors freezing;
— the hit pixel address readout time τ_{trig} to get the position of triggered pixels and to compute the pixels to be read;
— the readout time $\tau_{readout}$ to receive and encode one pixel data;
— the duration τ_{reset} of reset operation.

To read out N pixels, dead time is given by (1).

$$\tau_{deadtime} = \tau_{latency} + \tau_{trig} + N \cdot \tau_{readout} + \tau_{reset}. \quad (1)$$

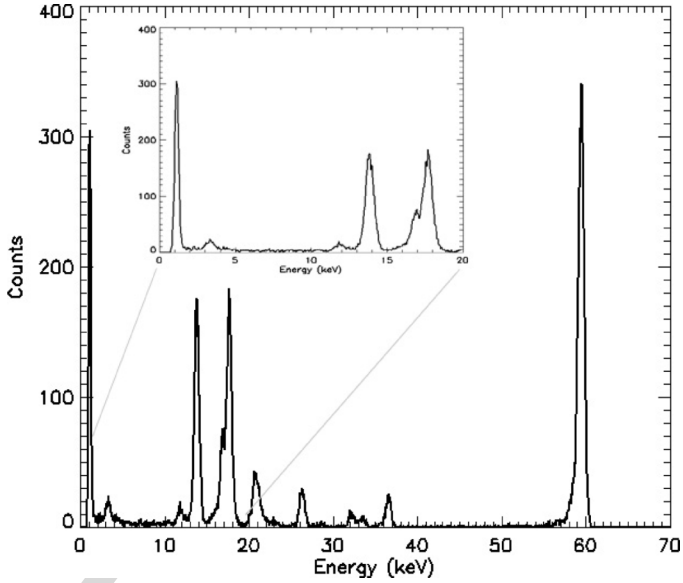

Fig. 11. Spectrum of pixel #1, for a detector cooled to $-10\,^{\circ}\mathrm{C}$ and biased at $-400\,\mathrm{V}$. Energy resolution is 650 eV FWHM at 13.9 keV and 796 eV FWHM at 59.54 keV. Multiple lines are visible on the left of the 17.75 keV peak. The 3.3 keV line is a source photon whereas the 1.2 keV structure corresponds to the noise rise and gives information about the low threshold of this pixel.

In Caliste 64, we measure that dead time can be as low as 30 μs to read one pixel when the peaking time is 9.6 μs. We have to add 1 μs per extra pixel to read ($\tau_{readout}$). With shorter peaking time, dead time can be reduced by configuring $\tau_{latency}$ and τ_{reset}.

D. Spectroscopy

When the camera is cooled down to $-10°\mathrm{C}$ (the lowest temperature currently achievable with our setup) and biased at $-400\,\mathrm{V}$, best spectroscopy results are obtained with a peaking time of 9.6 μs. According to Fig. 7, that proves that dark current is less than 5 pA per pixel at this temperature, which is consistent with current measured previously with detectors of this kind (Fig. 3).

The 64 pixels of the Caliste 64 prototype show excellent spectral quality. A typical spectrum obtained on one channel is shown Fig. 11. As there is no screen between the source and the detector, we can detect low energy photons, even an M X-ray fluorescence line of Neptunium, daughter of Americium, at 3.3 keV. From the noise rise on the left, we estimate that the low threshold is around 1.5 keV over the 64 channels. In the following spectra, we set the threshold value to ~ 2 keV in order to eliminate the noise rise. For instance, the energy resolution obtained from the pixel #1 of the matrix is 650 eV FWHM at 13.9 keV and 796 eV FWHM at 59.54 keV.

From the 64 spectra linearly calibrated in energy, we built a sum spectrum. Fig. 12 is the sum spectrum taking into account every event during 10 minutes. We measure an energy resolution of 808 eV FWHM at 60 keV and 697 eV FWHM at 14 keV. The 808 eV FWHM at 60 keV corresponds to an ENC of 58 electrons rms, in good agreement with electronics tests. Peak to valley ratio on the 60 keV line is very high and background between 36 keV and 60 keV is still flatter than on previous spectra (Fig. 5). In Fig. 13, multiple pixel interactions are removed from the

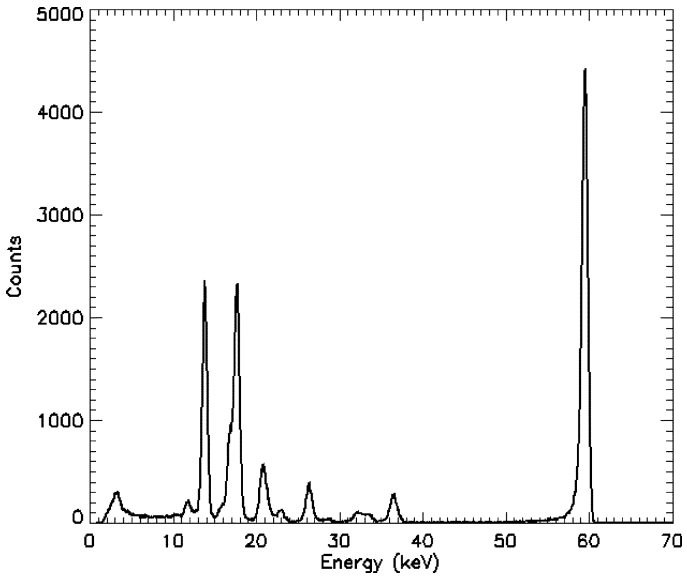

Fig. 12. Sum spectrum with Caliste 64 at $-10°\mathrm{C}$, $-400\ \mathrm{V}$, with a $^{241}\mathrm{Am}$ source and a peaking time of 9.6 μs. All the pixels contribute to the sum. Energy resolution is 697 eV FWHM at 13.9 keV and 808 eV FWHM at 59.54 keV. Peak to valley ratio between 59.54 keV peak and 57 keV is 62.

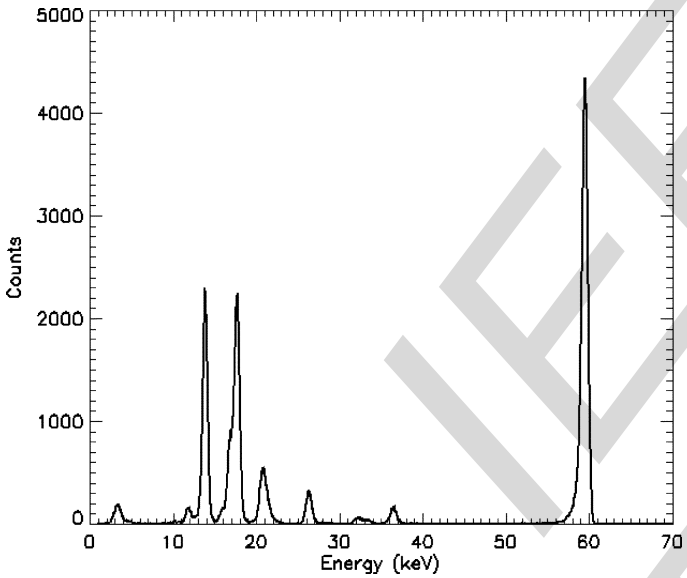

Fig. 13. Sum spectrum with Caliste 64 at $-10°\mathrm{C}$, $-400\ \mathrm{V}$, with a $^{241}\mathrm{Am}$ source and a peaking time of 9.6 μs. Only the single events are considered. All the pixels contribute to the sum. Energy resolution is 701 eV FWHM at 13.9 keV and 805 eV FWHM at 59.54 keV. Peak to valley ratio between 59.54 keV peak and 57 keV is 100.

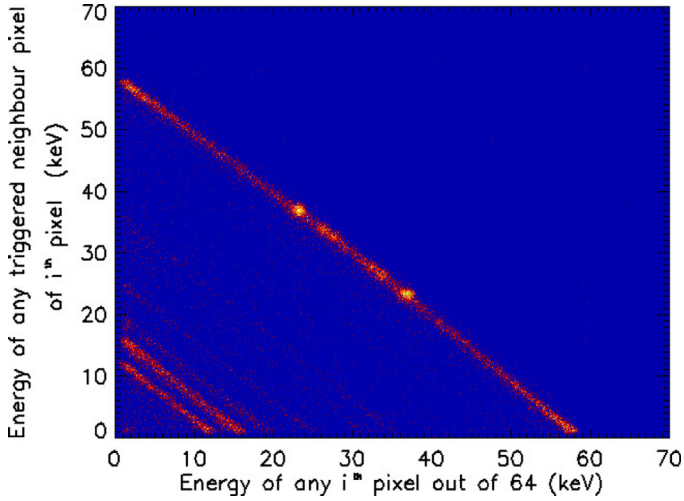

Fig. 14. Scatter plot of correlation of the energies of any couple of neighbor pixels that triggered at the same time. The sum of the two energies gives the energy of the incident photon.

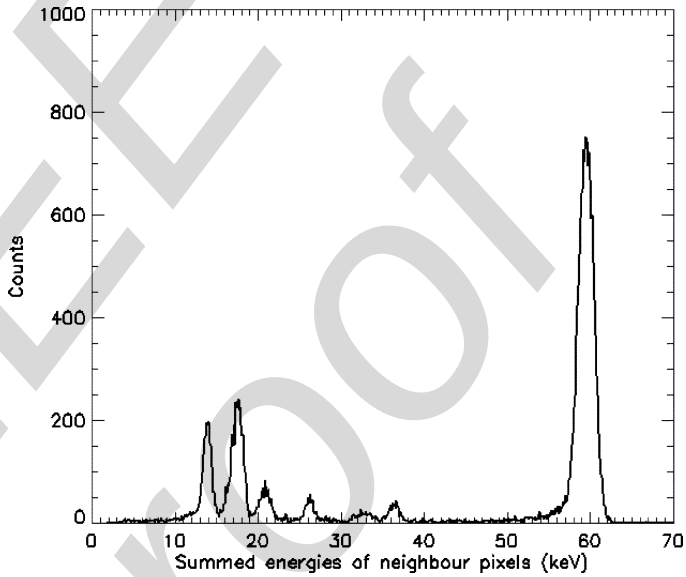

Fig. 15. Spectrum built by adding the energies of all the neighbor pixels that triggered at the same time. Even in case of charge sharing, we can find the energy of incident photon.

previous spectrum. The peak to valley ratio at 60 keV increases from 62 to 100 whereas the background becomes flat between 3 and 10 keV. Indeed, that operation suppresses all split events due to charge sharing or photon escape.

We studied the correlation between the energy of a pixel interaction $\#i$ with its neighbor $\#j$ for coincident events. The scatter plot of Fig. 14 shows a strong linear correlation, indicative of split event and charge sharing phenomena without charge loss in the gap between the pixels. The sum of the two energies only gives singular constants, which correspond to the energies of the Americium photons. Considering the 60 keV line, we observe an accumulation near 23 keV and 27 keV (and symmetrically 33 and 37 keV). These hot-spots are due to the X-Ray fluorescence photons escaping a pixel and stopping in the neighbor pixel. For instance, a 60 keV photon may interact firstly on a K-shell electron of a Cd atom. Consequently, a 23 keV K_α X-ray fluorescence photon is emitted from the Cd atom and may escape the pixel and reach the neighbor. These events are always detected in coincidence. We can notice that the 23 keV and the 27 keV lines vanished in the sum spectrum selecting only single events (Fig. 13).

We built a spectrum by adding the energies of the pixels $\#i$ and their neighbors $\#j$. The resulting calibrated spectrum shows an energy resolution of 1.2 keV FWHM at 14 keV and 2.1 keV FWHM at 60 keV (Fig. 15). These values are slightly

higher than expected when combining the noise of two independent channels. This effect is due to the linear calibration technique, which looks insufficient. Non-linear calibration will be implemented in future work. Anyway, the capability to find the incident energy of a photon interacting in-between two pixels proves that our detector with a segmented electrode is sensitive between the pixels.

V. Conclusion

We demonstrate excellent performance of an innovative micro hard-X ray camera with 64 pixels, based on a 3D Plus technology. The modular design allows single cameras to be juxtaposed into a large area and compact focal plane for the Simbol-X space mission. The first fully integrated Caliste 64 camera has 64 operating pixels and a very good spectral resolution, about ~ 700 eV FWHM at 14 keV and ~ 800 eV FWHM at 60 keV. Moreover, full energy reconstruction is easily achieved in the case of multiple pixel events.

Time resolution is better than 100 ns rms after the time-walk correction. Timing constraints in the Simbol-X mission come from the anticoincidence treatment for high energy particles (protons essentially). In that case, a 50 ns rms resolution can be reached with Caliste 64.

The next generation of Caliste is called Caliste 256. It will integrate 256 pixels of 625 μm pitch instead of 1 mm pitch. Detector geometry and hence, spatial resolution will be representative of the High Energy Detector of Simbol-X.

References

[1] P. Ferrando *et al.*, "SIMBOL-X: mission overview," *Proc. SPIE*, vol. 6266, 2006.

[2] G. Pareschi and P. Ferrando, "The SIMBOL-X hard X-ray mission," *Exp. Astron.*, vol. 20, no. 1–3, pp. 139–149, 2005.

[3] J. Treis *et al.*, "DEPFET based focal plane instrumentation for X-ray imaging spectroscopy in space," in *Proc. IEEE Nuclear Science Symp. Conf. Rec.*, Honolulu, HI, 2007, pp. 2226–2235.

[4] B. P. F. Dirks *et al.*, "The focal plane of the SIMBOL-X space mission," *Proc. SPIE*, vol. 6276, 2006.

[5] S. Watanabe *et al.*, "New CdTe pixel gamma-ray detector with pixelated Al Schottky anodes," *Jpn. J. Appl. Phys.*, vol. 46, pp. 6043–6043, 2007.

[6] C. Val and M. Leroy, "3D Plus," Patent 90 15473, Dec. 1990.

[7] H. Toyama *et al.*, "Formation of aluminium Schottky contact on plasma-treated cadmium telluride surface," *Jpn. J. Appl. Phys.*, vol. 43, pp. 6371–6375, 2004.

[8] H. Toyama *et al.*, "Effect of He plasma treatment on the rectification properties of Al/CdTe Schottky contacts," *Jpn. J. Appl. Phys.*, vol. 44, pp. 6742–6746, 2005.

[9] T. Takahashi and S. Watanabe, "Recent progress in CdTe and CdZnTe detectors," *IEEE Trans. Nucl. Sci.*, vol. 48, no. 4, pp. 950–959, Aug. 2001.

[10] F. Lugiez *et al.*, "IDeF-X V1.1: Performances of a new CMOS 16 channels analogue readout ASIC for Cd(Zn)Te detectors," in *Proc. IEEE Nuclear Science Symp. Conf. Rec.*, San Diego, CA, 2006, vol. 2, pp. 841–844.

[11] B. P. F. Dirks *et al.*, "Leakage current measurements on pixelated CdZnTe detectors," *Nucl. Instrum. Methods Phys. Res. A*, vol. A567, pp. 145–149, 2006.

[12] O. Gevin *et al.*, "IDeF-X V1.0: Performances of a new CMOS multi channel analogue readout ASIC for Cd(Zn)Te detectors," in *Proc. IEEE Nuclear Science Symp. Conf. Rec.*, Las Croabas, Puerto Rico, 2005, pp. 433–437.

[13] H. Toyama *et al.*, "Analysis of polarization phenomenon and deep acceptor in CdTe radiation detector," in *Proc. IEEE Nuclear Science Symp. Conf. Rec.*, San Diego, CA, 2006, vol. 6, pp. 3694–3699.